24th INTERNATIONAL CONGRESS ON SOUND AND VIBRATION
23–27 July 2017, London

ICSV24
23-27JULY 2017
LONDON CALLING

DAMPING DUE TO THE ACOUSTIC BOUNDARY LAYER IN HIGH-FREQUENCY TRANSVERSE MODES

Pedro Romero[1], Tobias Hummel[1,2], Frederik M. Berger[1], Bruno Schuermans[2,3] and Thomas Sattelmayer[1]

[1] *Lehrstuhl für Thermodynamik, Technische Universität München, D-85748 Garching, Germany*

[2] *Institute for Advanced Study, Technische Universität München, D-85748 Garching, Germany*

[3] *GE Power, Baden, Switzerland*

email: romero@td.mw.tum.de

In gas turbine combustors, thermoacoustic instabilities arise when the flame's unsteady heat release couples to the combustor acoustics and the resulting feedback loop transfers more energy to the acoustic field than it is dissipated by the damping mechanisms. One of these damping mechanisms are the viscous losses within the acoustic boundary layer. This paper presents a model that describes these losses, which can be implemented as a boundary condition in the acoustic governing equations, capturing the dampening effect of the acoustic viscous boundary layer without numerically resolving it. This allows to determine damping rates of generic three-dimensional geometries and mode shapes, including the transverse modes that appear beyond the cut-off frequency. The derived model is tested for the first transverse mode against damping rates measured in an experimental test rig. For that purpose, the eigenvalue problem of the Helmholtz equation –including the boundary layer boundary condition– is numerically solved and the damping rate is obtained from the imaginary part of the complex eigenfrequency.

Keywords: acoustic boundary layer, damping rate, high-frequency thermoacoustic instabilities

1. Introduction

Current gas turbine combustors, which are based on lean premixed technologies, tend to develop thermoacoustic instabilities that can restrict their operational range and increase pollutant emissions [1]. According to the extended Rayleigh criterion [2], an instability arises if driving –i.e. constructive coupling between the flame's unsteady heat release and the chamber acoustics– exceeds the acoustic damping, e.g. losses through open boundaries, interactions between acoustics and mean flow, energy dissipation in the boundary layer. Therefore, in order to computationally predict whether a combustor becomes unstable, an accurate description of both driving and damping is needed. Although over the past decades advances have been made in the comprehension and prediction of low-frequency pulsations, the high frequency range remains not completely understood [3]. Direct numerical simulation of thermoacoustic instabilities is far beyond current computing power, and even though transient CFD simulations like LES are possible, their associated high computational cost prevents using them as a dynamic design tool. Taking advantage of the scale disparity of the acoustic motion compared to the steady mean flow, more time-efficient approaches use the Linearized Euler (LEE) or Linearized Navier-Stokes equations (LNSE) in frequency domain to describe the linear stability limits of gas turbine combustors [4]. In these methods, the linear driving potential introduced by the flame can be described by means of Flame Transfer Functions (FTF) [5], which relate the flame's unsteady heat release to acoustic fluid variables. Regarding damping, LEE and LNSE intrinsically capture the losses arising from interactions between the acoustic field and the mean flow. Furthermore, as long as one is working in frequency domain, open boundaries can be cast into impedances or reflection coefficients, which can be easily implemented as boundary conditions in the equations. The acoustic boundary layer is usually neglected in such acoustic approaches as it has a negligible effect on the acoustic propagation [6] –i.e. mode shapes. However it is known from studies carried out on tubes that the boundary layer may have a non-negligible effect on the damping rates. For example in [7], the author derives an analytic formula to assess the damping rate due to the boundary layer for one-dimensional

modes within a hard-walled tube[1]. In that formula, for a given thermodynamic state of a gas, the damping rate grows linearly with the surface-to-volume ratio and proportionally to the square root of the frequency. In other words, for flat combustors –i.e. high surface-to-volume ratio– and/or high frequencies the acoustic losses due to the boundary layer can play a role on the damping rate. The damping due to the acoustic boundary layer can be allocated to thermal and to viscous effects, i.e. thermal and viscous acoustic boundary layers. The scalar character of the temperature allows to model the diffusion within the thermal boundary layer as an impedance [8]. However, the velocity is a vector for the transverse modes, therefore its diffusion depends on its local direction precluding to cast the viscous effects into an impedance.

This paper introduces a model that takes into account the acoustic viscous boundary layer, without directly resolving it, and which can be implemented as a boundary condition in the acoustic governing equations. The main novelty of the model hereby presented is that it allows to assess the damping rates of generic three-dimensional mode shapes and geometries, and thus it is suitable for studying high frequency thermoacoustic instabilities.

This work is structured as follows. First, theoretical background is presented, therein a one-dimensional model for the boundary layer losses is derived and subsequently extended to three-dimensional cases. Second, a validation of both models is carried out. The one-dimensional model is compared to analytic results and the three-dimensional model is validated against experimental measurements. Conclusions and next steps are summarized in the last section.

2. Theoretical Background

In this section, the viscous boundary layer losses model is presented. Firstly, a boundary condition for one-dimensional (1D) acoustics is derived. In that regard, the linearized Navier-Stokes equations are solved under suitable assumptions to obtain such a boundary condition. Secondly, the 1D model is extended to three-dimensions (3D). Specifically, it is proved that the 1D model can be applied to 3D in local curvilinear coordinates. Therefore, in a last step, transforming the 1D model from curvilinear to cartesian coordinates, the generic 3D boundary condition is obtained.

2.1 Derivation of a One-Dimensional Model for Viscous Losses within the Boundary Layer

To describe the acoustics in engineering applications such as gas turbines, the Navier-Stokes equations are simplified under the assumption of small harmonic acoustic oscillations of angular frequency ω, yielding the linearized Navier-Stokes equations in frequency domain [9]:

$$\mathrm{i}\omega\hat{\rho} + \nabla\cdot(\hat{\rho}\mathbf{u}_0) + \nabla\cdot(\rho_0\hat{\mathbf{u}}) = 0, \tag{1}$$

$$\mathrm{i}\omega\rho_0\hat{\mathbf{u}} + \hat{\mathbf{u}}\cdot\nabla\mathbf{u}_0 + \mathbf{u}_0\cdot\nabla\hat{\mathbf{u}} = -\nabla\hat{p} + \mu\nabla^2\hat{\mathbf{u}}, \tag{2}$$

$$\mathrm{i}\omega\hat{p} + \mathbf{u}_0\cdot\nabla\hat{p} + \hat{\mathbf{u}}\cdot\nabla p_0 + \gamma\left(p_0\nabla\cdot\hat{\mathbf{u}} + \hat{p}\nabla\cdot\mathbf{u}_0\right) = -\nabla\cdot\hat{\mathbf{q}}. \tag{3}$$

Density, pressure and the vector velocity are denoted by ρ, p and $\mathbf{u}$, respectively. The subscript $(\cdot)_0$ stands for the mean flow variables, while the hat $(\hat{\cdot})$ designates complex amplitudes of acoustic variables. The heat capacity ratio and the dynamic viscosity are designated by γ and μ, respectively. Finally, the heat flux is denoted by $\hat{\mathbf{q}}$. In the acoustic motion near to solid boundaries, as in the classical boundary layer theory, two zones can be distinguished: one far from the solid boundaries, where there is an ideal acoustic flow with negligible viscous effects, and another close to the solid boundaries where viscosity effects come into play. The latter is the so-called acoustic boundary layer [10].

The velocity profile of a two-dimensional acoustic boundary layer is depicted in Fig. 1. Note that outside that boundary layer the motion is simply one-dimensional ideal flow, whilst within the boundary layer the velocity decreases until fulfilling the no-slip condition at the wall. In order to obtain the expression for the acoustic quantities within the boundary layer, some assumptions are made on Eqs. (1)-(3):

i) The mean flow is neglected[2], i.e. $\mathbf{u}_0 = 0$

ii) No heat flux through the wall is considered, i.e. $\hat{\mathbf{q}} = 0$, only dissipation due viscous efforts is taken into account. Thermal effects are left aside as they can be separately modeled with an acoustic impedance [8]

[1] see Eq. (26) in Section 3.1 of this paper

[2] This is a reasonable assumption since the hydrodynamic boundary layer is much thicker than the acoustic boundary layer

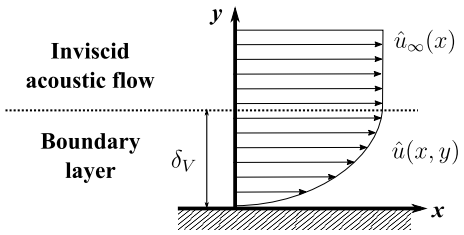

Figure 1: Schematic of a 2D acoustic boundary layer

iii) Spatially constant mean pressure as within the hydrodynamic boundary layer, i.e. $\nabla\hat{p} = 0$

As a result, the simplified version of Eqs. (1)-(3) yields

$$\mathrm{i}\omega\hat{\rho} + \nabla\cdot(\rho_0\hat{\mathbf{u}}) = 0, \tag{4}$$

$$\mathrm{i}\omega\rho_0\hat{\mathbf{u}} = -\nabla\hat{p} + \mu\nabla^2\hat{\mathbf{u}}, \tag{5}$$

$$\mathrm{i}\omega\hat{p} + \gamma\,(p_0\nabla\cdot\hat{\mathbf{u}}) = 0. \tag{6}$$

The boundary layer represents a very thin zone of thickness $\delta_V = \sqrt{2\nu/\omega}$, being $\nu = \mu/\rho_0$ the kinematic viscosity, in the direction normal to the wall (y-direction in Fig. 1). Such a thickness, which is the length scale in y-direction, is very small compared to the acoustic wavelength (λ), which is the length scale in x-direction[3]. Consequently, an order of magnitude analysis can be carried out, and spatial variations –i.e. gradients– in directions parallel to the wall can be neglected, further simplifying Eqs. (4)-(6):

Equations	Acoustic Viscous Boundary Layer		Inviscid Acoustic Flow	
Continuity	$\mathrm{i}\omega\hat{\rho} + \rho_0\left(\dfrac{\partial\hat{u}}{\partial x} + \dfrac{\partial\hat{v}}{\partial y}\right) = 0$	(7)	$\mathrm{i}\omega\hat{\rho}_\infty + \rho_0\,\dfrac{\partial\hat{u}_\infty}{\partial x} = 0$	(11)
X-momentum	$\mathrm{i}\omega\rho_0\hat{u} = -\dfrac{\partial\hat{p}}{\partial x} + \mu\dfrac{\partial^2\hat{u}}{\partial y^2}$	(8)	$\mathrm{i}\omega\rho_0\hat{u}_\infty = -\dfrac{\partial\hat{p}_\infty}{\partial x}$	(12)
Y-momentum	$\dfrac{\partial\hat{p}}{\partial y} = 0$	(9)	–	
Energy	$\mathrm{i}\omega\hat{p} + \gamma p_0\left(\dfrac{\partial\hat{u}}{\partial x} + \dfrac{\partial\hat{v}}{\partial y}\right) = 0$	(10)	$\hat{p}_\infty = c_0^2\,\hat{\rho}_\infty$	(13)

Equations (7)-(10) describe the acoustic flow within the boundary layer. There, $\hat{u}$ and $\hat{v}$ represent complex acoustic amplitudes of the velocity in x- and y-directions, respectively. The governing equations of the one-dimensional inviscid flow outside the boundary layer, Eqs. (11)-(13), are obtained from Eqs. (7)-(10) setting μ and $\hat{v}$ to zero. In that set, the subscript $(\cdot)_\infty$ designates the variables outside the boundary layer. Furthermore, c_0 stands for the speed of sound. Finally, note that a momentum equation in y-direction does not exist outside the boundary layer because of the unidimensionality of the motion.

Equation (9) implies that the pressure throughout the boundary layer is constant and equal to its value outside the boundary layer, i.e. $\hat{p} = \hat{p}_\infty(x)$. Therefore, pressure can be written overall as a function of the acoustic velocity outside the boundary layer, $\hat{u}_\infty(x)$, using Eq. (12). Specifically, by doing so in Eq. (8), a differential equation for $\hat{u}$ is obtained

$$\mathrm{i}\omega\rho_0\,(\hat{u} - \hat{u}_\infty) = \mu\frac{\partial^2\hat{u}}{\partial y^2}. \tag{14}$$

Equation (14) can be integrated applying proper boundary conditions: zero velocity at the wall, i.e. $\hat{u}(0) = 0$ and the velocity of the inviscid acoustic flow at the upper edge of the boundary layer, i.e. $\hat{u}(\infty) = \hat{u}_\infty(x)$. Consequently, after integrating Eq. (14), the velocity profile of $\hat{u}$ yields

$$\hat{u} = \hat{u}_\infty(x)\left[1 - \mathrm{e}^{-(1+i)\frac{y}{\delta_V}}\right]. \tag{15}$$

[3] The boundary layer thickness compared to the acoustic wavelength is $\delta_V/\lambda \approx \sqrt{\omega\nu}/c_0$, for gases they only reach the same order of magnitude for extremely high frequencies $\omega \approx 10^{10}\mathrm{rad\ s^{-1}}$

To obtain the density distribution within the boundary layer, the energy and continuity equations, Eqs. (7) and (10), can be combined by equaling the divergence of velocity. After some mathematical manipulation, the isentropic relation (13) is recovered and thus it applies within the viscous boundary layer too. As a result, the density is directly proportional to the pressure and, like the pressure, it keeps the same value as outside the boundary layer, i.e. $\hat{\rho} = \hat{\rho}_\infty(x)$. To determine the last unknown of the problem, the velocity in y-direction ($\hat{v}$), Eq. (7) is used. Inserting Eq. (13) and Eq. (15) into Eq. (7) results in

$$\underbrace{\mathrm{i}\omega\frac{\hat{\rho}_\infty(x)}{\rho_0} + \frac{\mathrm{d}\hat{u}_\infty(x)}{\mathrm{d}x}}_{=0} = \frac{\mathrm{d}\hat{u}_\infty(x)}{\mathrm{d}x}\mathrm{e}^{-(1+\mathrm{i})\frac{y}{\delta_V}} - \frac{\partial\hat{v}}{\partial y}, \tag{16}$$

where the left hand side of the previous expression can be identified as the continuity equation outside the boundary layer, Eq. (11), which equals to zero. As a result, a differential equation for $\hat{v}$ is obtained. The boundary condition at the wall is again zero velocity, $\hat{v}(0) = 0$, so integrating Eq. (16), the following expression is obtained

$$\hat{v}(x,y) = -\sqrt{\frac{\nu}{\mathrm{i}\omega}}\frac{\mathrm{d}\hat{u}_\infty(x)}{\mathrm{d}x}\left[\mathrm{e}^{-(1+\mathrm{i})\frac{y}{\delta_V}} - 1\right]. \tag{17}$$

Equation (17) describes the $\hat{v}$-velocity distribution within the boundary layer. When y tends to infinity, the value of the normal velocity at the upper edge of the boundary layer is recovered

$$\hat{v}_\infty(x) = \sqrt{\frac{\nu}{\mathrm{i}\omega}}\frac{\partial\hat{u}_\infty}{\partial x}. \tag{18}$$

Equation (18) can be implemented as a boundary condition ($\hat{\mathbf{u}}\cdot\mathbf{n} = \hat{v}_\infty$) to one-dimensional inviscid acoustic flows. Compared to the usual slip condition $\hat{\mathbf{u}}\cdot\mathbf{n} = 0$, which imposes acoustic hard walls –i.e. no acoustic flow going through the walls, the presence of the boundary layer implies a "softening" of the walls allowing some acoustic flux crossing them. That flux can be interpreted as loss of acoustic energy that causes attenuation of the acoustic waves. Finally, note that Eq. (18) depends solely on the acoustic ideal flow, for that reason one does not need to resolve the boundary layer, avoiding mesh refining near the boundaries. Consequently, the CPU times remain small.

2.2 Extension of the One-Dimensional Model to Three Dimensions

In the previous section a boundary condition for one-dimensional acoustics was obtained. Such a boundary condition cannot be employed for transverse modes because there, the acoustic velocity locally behaves as a three-dimensional vector. In this section, it is shown that locally, in curvilinear coordinates, the structure of the boundary layer is equivalent to a two-dimensional boundary layer like the one derived in the Section 2.1. Such a local representation cannot be directly applied in the acoustic governing equations. Therefore, a transformation from curvilinear coordinates to cartesian coordinates is carried out. As a result a generic model, which is applicable to universal thermoacoustic stability prediction tools, is obtained.

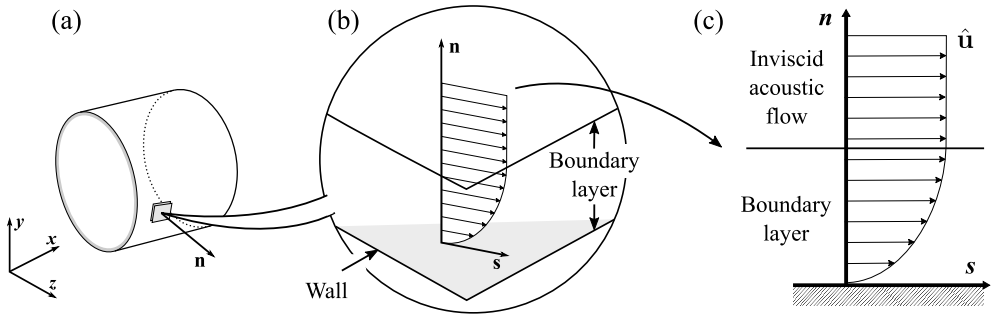

Figure 2: (a) Generic geometry (b) Flat boundary layer (c) Velocity profile within the boundary layer

The curvature of a typical combustor geometry is much larger than the boundary layer thickness [4]. Therefore, one can assume that the boundary layer is confined to a two-dimensional flat layer as depicted in Fig.2 (b). In

[4] Assuming $\nu \approx 10^{-5}$ m^{2}s^{-1}; $\omega \approx 10^3$ rad s^{-1} and the curvature $R_c \approx 10^{-2}$ m^{-1}, then $R_c/\delta_v \approx 10^2$

that two-dimensional framework, using a working plane defined by the normal to the chamber's surface ($\mathbf{n}$) and the direction of the acoustic velocity ($\mathbf{s}$), the boundary layer can be treated as a two-dimensional boundary layer, in the same way it was done in the Section 2.1. The difference between the one- and three-dimensional approaches lies in the coordinate systems employed: cartesian coordinates, x and y, for the one-dimensional problem and the curvilinear coordinates of the axes $\mathbf{n}$ and $\mathbf{s}$, i.e. n and s, for three dimensions. Specifically, n is equivalent to y and s to x, cf. Fig. 2 (c). Such an equivalence is mathematically proved next.
The continuity equation taking into account that the velocity is now a vector reads:

$$\mathrm{i}\omega\hat{\rho} + \rho_0 \left(\nabla_{\mathbf{n}} \cdot \hat{\mathbf{u}} + \nabla_{\mathbf{s}} \cdot \hat{\mathbf{u}}\right) = 0, \tag{19}$$

where the divergence operator is split into two: a normal divergence in n-direction ($\nabla_{\mathbf{n}}$) and a tangent divergence in s-direction ($\nabla_{\mathbf{s}}$). That separates the normal and tangential contributions, with the objective of integrating Eq. (19) in normal direction. Expanding the normal divergence as $\nabla_{\mathbf{n}} \cdot \hat{\mathbf{u}} = \partial \hat{u}_n / \partial n$, Eq. (19) can be integrated analogously to Eq. (16). Consequently, the normal velocity at the upper edge of the boundary layer yields:

$$\hat{u}_{n\infty}(s) = \sqrt{\frac{\nu}{\mathrm{i}\omega}} \left(\nabla_{\mathbf{s}} \cdot \hat{\mathbf{u}}_{\infty}\right). \tag{20}$$

In curvilinear coordinates the velocity outside the boundary layer can be expressed as $\hat{\mathbf{u}}_{\infty} = |\hat{\mathbf{u}}_{\infty}|\ \mathbf{s}$, where $|\hat{\mathbf{u}}_{\infty}|$ is the magnitude of the complex velocity vector, which in turn is a scalar function of s. Then, expanding the divergence in tangential direction, Eq. (20) yields

$$\hat{u}_{n\infty}(s) = \sqrt{\frac{\nu}{\mathrm{i}\omega}} \frac{\partial |\hat{\mathbf{u}}_{\infty}|}{\partial s}, \tag{21}$$

which is an analogous expression derived in the one-dimensional case, Eq. (18). Nevertheless, Eq. (21) is still a function of the local curvilinear coordinate s. Then, the coordinate transformation to cartesian coordinates is carried out by using the chain rule as follows:

$$\frac{\partial |\hat{\mathbf{u}}_{\infty}|}{\partial s} = \frac{\partial |\hat{\mathbf{u}}_{\infty}|}{\partial x}\frac{\partial x}{\partial s} + \frac{\partial |\hat{\mathbf{u}}_{\infty}|}{\partial y}\frac{\partial y}{\partial s} + \frac{\partial |\hat{\mathbf{u}}_{\infty}|}{\partial z}\frac{\partial z}{\partial s} = \nabla |\hat{\mathbf{u}}_{\infty}| \cdot \mathbf{s}, \tag{22}$$

where the partial derivative with respect to s is written in terms of the gradient of the magnitude of the acoustic velocity and the curvilinear basis vector $\mathbf{s}$. Both quantities are expressed in cartesian coordinates, particularly the vector $\mathbf{s}$, which is the direction of the velocity, can be written as $\mathbf{s} = \hat{\mathbf{u}}_{\infty}/V$. As a result, the normal velocity at the upper edge of the boundary layer, expressed in cartesian coordinates yields

$$\hat{u}_{n\infty}(\mathbf{x}) = \sqrt{\frac{\nu}{\mathrm{i}\omega}} \left(\frac{\nabla |\hat{\mathbf{u}}_{\infty}| \cdot \hat{\mathbf{u}}_{\infty}}{|\hat{\mathbf{u}}_{\infty}|}\right). \tag{23}$$

Equation (23) represents a boundary condition that can be implemented in the thermoacoustic stability prediction tools.

3. Validation of the Models

In this section the derived models are validated. Firstly, the verification of the one-dimensional boundary condition is conducted against analytic benchmarks, as they are readily available from the literature. Secondly, the extended three-dimensional boundary condition is validated against an experimental test case.

3.1 Validation of the One-Dimensional Model against Analytic Baselines

In this section, the validation of the one-dimensional boundary condition derived in Section 2.1 is carried out. For that purpose, the attenuated acoustic field within a straight tube is computed. Firstly, a pressure response study the attenuation of the acoustic pressure waves is conducted and compared to an analytic dispersion relation. Secondly, an eigenvalue (EV) study is conducted and the damping rate, which is the imaginary part of the eigenfrequency, is compared to analytic benchmarks.
A tube of $1\ \mathrm{m}$ length by $0.1\ \mathrm{m}$ radius is employed as test case (cf. Fig 3 (a)). Constant bulk pressure and temperature are set to $101,325\ \mathrm{Pa}$ and $300\ \mathrm{K}$, respectively. The corresponding kinematic viscosity at $300\ \mathrm{K}$ is increased by a factor 200 up to $3.14 \times 10^{-3}\ \mathrm{m^2\,s^{-1}}$ in order to induce noticeable attenuation in the pressure

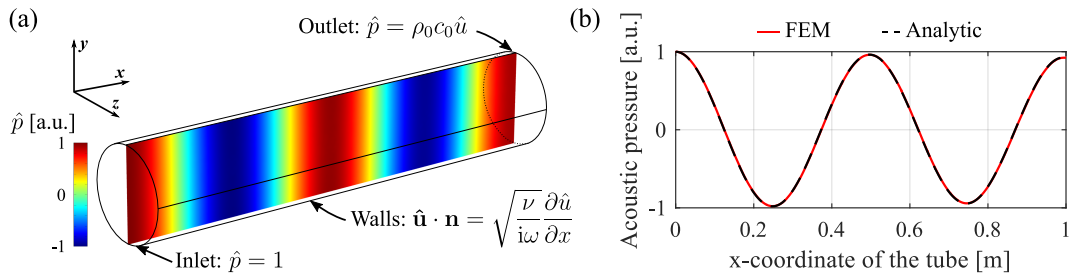

Figure 3: (a) Geometry and acoustic pressure (b) Spatial pressure trace from FEM (red solid), analytic solution from dispersion relation Eq. (25) (black dashed)

traces. The acoustic field is described by means of a three-dimensional Helmholtz system (cf. Eqs. (4)-(6) with $\mu = 0$). Such a system is solved using a Finite Element Method (FEM) scheme. The computational domain is discretized using an unstructured tetrahedral mesh with a spatial resolution of approximately 13 cells per wavelength. Quadratic Lagrange functions are used as weighting functions in the FEM scheme, which turns out in approximately 35,500 degrees of freedom (DOF).

First, the pressure response study is carried out. At the inlet, the pressure is set to 1 to act as longitudinal excitation, (cf. Fig. 3 (a)). At the outlet, $\hat{p} - \rho_0 c_0 \hat{u} = 0$ is applied. That represents a non-reflecting boundary condition, which was chosen to have a clearer pressure response without interference from the reflected waves at the outlet as well as being consistent with the analytic solution. At the walls, to include the boundary layer effect, Eq. (18) is used. Then, the Helmholtz system is solved for a frequency of 694 Hz (third longitudinal mode of the tube)[5]. The one-dimensional pressure field is depicted in Fig. 3 (b), where one can recognize a slightly attenuation between the inlet and the outlet of the tube. In order to assess the accuracy of the computed attenuated pressure trace, it is compared to its analytic solution. For a longitudinal mode within a tube, the pressure obeys [8]:

$$\hat{p}_{an}(x) = \mathrm{Re}\{\hat{p}_0 \exp(\mathrm{i}k_x x)\} \tag{24}$$

where $\hat{p}_0$ and k_x denote the pressure amplitude and the longitudinal wavenumber, respectively. For the tube, the latter can be written in terms of the following relation that takes into account viscous losses [8]:

$$\frac{k_x^2}{k_0^2} = \frac{A}{A - \frac{1}{2}(1-\mathrm{i})L_p\delta_V}, \tag{25}$$

where A and L_p are the cross-sectional area and perimeter of the tube, respectively. In addition, k_0 is the unperturbed wavenumber defined as $k_0 = \omega/c_0$. Using Eqs. (24) and (25), with $\hat{p}_0$ equals to 1, the analytic pressure distribution is plotted in Fig. 3 (b). One can observe that there is an almost perfect match between the analytic and the computed pressure traces. This similarity is confirmed by calculating the 2-norm relative error between both curves, $||\hat{p}_{an}(x) - \hat{p}_{FEM}(x)||_2 / ||\hat{p}_{an}(x)||_2$. It renders an error of 0.77 %, ensuring that a correct attenuation is captured by the numerical model.

Second, an EV study is carried out to assess the damping rates due to the viscous boundary layer. From an EV study are retrieved complex eigenvectors and eigenfrequencies. On the one hand, the eigenvectors represent the shape of the oscillating mode. On the other hand, the real part of the eigenfrequency is the oscillation frequency of the mode, while the imaginary part corresponds to the damping rate of that particular mode, i.e. $\omega = \omega_R + \mathrm{i}\alpha$. Again the three-dimensional Helmholtz system is numerically solved via FEM. The same mesh as for the pressure response study is employed. At the walls Eq. (18) is applied. At the inlet and outlet zero acoustic velocity is set ($\hat{u} = 0$) to be consistent with the boundary conditions implemented on the analytic model used for validation purposes. The value of the computed damping rate for the third longitudinal mode is given in Table 1. As analytic baseline, the expression for assessing the decay in tubes introduced in [7] is used

$$\alpha = \frac{1}{R_t}\sqrt{\frac{\nu\omega}{2}}, \tag{26}$$

being R_t the radius of the tube. The value of the analytic damping rate is listed in Table 1. One can observe that the relative error between the analytic and the numerical damping rates remains below 2 %, proving that

[5]The election of that particular mode attends to purely illustrative reasons, as similar errors are obtained for all the other modes

the derived boundary condition precisely reproduces damping rates. Overall, as the three-dimensional model is obtained from a mathematical transformation from this model, the accuracy obtained can be extrapolated for the extended model too.

Table 1: Comparison of analytic and numerical damping rates

	Analytic Eq. (26)	Numerical FEM	Abs. Error [%]
Damping rates [rad s^{-1}]	26.16	26.56	1.5

3.2 Validation of the Three-Dimensional Model against an Experimental Test Case

In this section, the validation of the generic boundary condition derived in Section 2.2 is carried out. In that regard, the damping rate of the first transverse (T1) mode of the Common Research Chamber (CRC) [11] is computed. Subsequently, the simulated damping rate is compared to readily available measured damping rates. The CRC is a test rig located at the DLR in Lampoldshausen and dedicated to study high-frequency combustion instabilities. Geometrically, the test rig consists of a cylindrical combustion chamber with 0.2 m in diameter and 0.04 m in depth (cf. Fig. 4 (a)). Before conducting reactive experiments, the combustion chamber was acoustically characterized under cold-flow conditions. Specifically, the forced response at $1,000$ Hz, which corresponds to the T1 mode of the chamber (cf. Fig. 4 (b)), was measured and the damping rate identified from the power spectrum of the signal [11]. As long as there was no mean flow in the chamber, the damping was found to be mainly due to the viscous and thermal diffusion within the boundary layers.

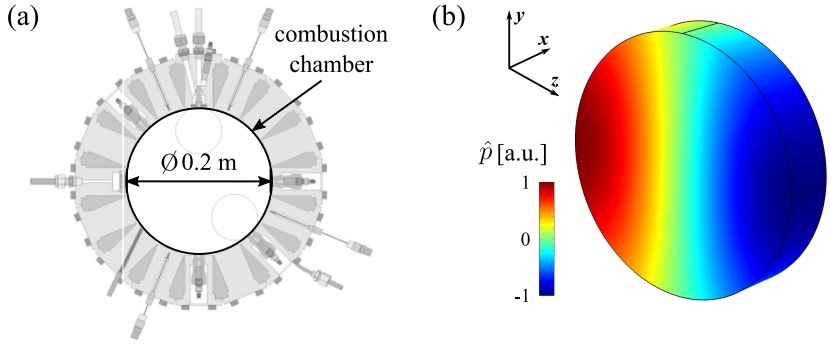

Figure 4: (a) Cross section of the CRC (b) Computed acoustic pressure T1 mode

To compute the damping rate of the T1 mode of the chamber two eigenvalue (EV) studies are conducted. One is needed to assess the damping due to the viscous boundary layer, and the other for the damping due to the thermal boundary layer, for which, as stated in the Introduction, impedance models are readily available. Particularly, the following expression derived in [8] is employed:

$$Z_T = \frac{\hat{p}}{\rho_0 c_0 \hat{u}_n} = \rho_0 c_0 \frac{(1-\mathrm{i})c_0}{(\gamma-1)\omega\delta_T}, \tag{27}$$

where δ_T stands for the thermal boundary layer thickness, which is related to the viscous thickness through the Prandtl number (Pr) via $\delta_V = \delta_T\sqrt{\mathrm{Pr}}$. As the acoustic motions have been considered linear during the derivations, the total damping rate is obtained by simply adding both contributions. The total damping cannot be calculated in a single study because Eq. (23), which includes the viscous part, and Eq. (27), which considers the thermal part, both impose a condition on the same variable $\hat{u}_n$. Imposing two different conditions for the same variable at the same mesh element is not numerically consistent. Therefore, the studies for the thermal and viscous contributions have to be conducted separately. In each case, as in Section 3.1, the Helmholtz system is solved via FEM. The computational domain is discretized using an unstructured tetrahedral mesh with a resolution of approximately 40 cells per wavelength. Quadratic Lagrange weighting functions are again employed for a total of 103,400 DOF. Constant mean pressure and temperature are prescribed as $101,325$ Pa and 288.15 K, respectively. Consequently, the kinematic viscosity is 1.57×10^{-5} $\mathrm{m^2\,s^{-1}}$ and the Prandtl number 0.77. The Helmholtz system is solved and the computed damping rates are listed in the Table 2 along with the recorded CPU times (computed in a workstation with 8 cores at 3.4GHz; 16GB RAM).
The difference between the computed and experimental damping rates can be attributed to the detachment of the acoustic boundary layer at sharp edges, which is not included in the model. That would increase the damping

Table 2: Computed and experimental damping rates of the CRC

	EV Study: Viscous	EV Study: Thermal	Total	Experimental [11]
CPU time [s]	42	12	54	-
Damping rate [$\mathrm{rad\ s^{-1}}$]	6	3.8	9.8	13

near the corners due to the creation of zones of vortex shedding. Although a slight mismatch is found, the results are in good agreement with the experimental benchmarks. Furthermore, the CPU times measured are in the order of minutes. That allows to efficiently account for the damping due to the boundary layer since early design stages.

4. Conclusion

A generic three-dimensional boundary condition that accounts for the viscous losses within boundary layers was presented. Implemented in the governing acoustic equations, the boundary condition allows to calculate the damping rates due to the boundary layer in real combustor geometries featuring transverse acoustic modes. For validation purposes, the damping rate associated to the first transverse mode of a experimental combustor was computed. The results were compared to readily available measured damping rates. A good agreement was found, although a slight mismatch occurred. That small discrepancy can be ascribed to the vortex shedding that takes place when the acoustic boundary layer detaches near to sharp edges. That contribution is not captured by the current model and is left to future work.

Acknowledgments

The authors gratefully acknowledge the Deutches Zentrum für Luft- und Raumfahrt (DLR) for providing the measured damping rates of the CRC. Financial support is provided by the Technische Universität München - Institute for Advanced Study funded by the German Excellence Initiative. The investigations were conducted as part of the joint research program COOREFLEX-Turbo in the frame of AG Turbo. The work was supported by the Bundesministerium für Wirtschaft und Technologie (BMWi) as per resolution of the German Federal Parliament under grant number 03ET7021T. The authors gratefully acknowledge AG Turbo and GE Power for their support and permission to publish this paper. The responsibility for the content lies solely with its authors.

REFERENCES

1. Sattelmayer, T., *Grundlagen der Verbrennung in stationären Gasturbinen*, Ch. 9 in: Stationäre Gasturbinen, Springer Verlag, (2010).
2. Chu, B. T., On the energy transfer to small disturbances in fluid flow (I), Acta Mechanica, (1965).
3. O'Connor, J.; Acharya, V.; Lieuwen, T., Transverse combustion instabilities: Acoustic, fluid mechanic, and flame processes, *Progress in Energy and Combustion Science*, **49**, (2015).
4. Schulze, M.; Hummel, T.; Klarmann, N.; Berger, F.; Schuermans, B.; Sattelmayer, T., Linearized Euler Equations for the Prediction of Linear High-Frequency Stability in Gas Turbine Combustors, *Proc. of the ASME Turbo*, (2016).
5. Hummel, T.; Berger, F. M.; Hertweck, M.; Schuermans, B.; Sattelmayer, T., High-Frequency Thermoacoustic Modulation Mechanisms in Swirl-Stabilized Gas Turbine Combustors Part Two: Modeling and Analysis, *Journal of Engineering for Gas Turbines and Power*, (2017).
6. Gikadi, J.; Schulze, M.; Schwing, J.; Föller, S.; Sattelmayer, T., Linearized Navier-Stokes and Euler Equations for the Determination of the Acoustic Scattering Behaviour of an Area Expansion, *18th AIAA/CEAS Aeroacoustics Conference*, AIAA-2012-2292, (2012).
7. Culick, F.E.M., Unsteady Motions in Combustion Chambers for Propulsion Systems, pp. 5-28, Technical Report AG-AVT-039, RTO of NATO, (2006).
8. Rienstra, S.W.; Hirschberg, A., *An Introduction to Acoustics*, pp. 76-81, (2004).
9. Gikadi, J., Prediction of Acoustic Modes in Combustors using Linearized Navier-Stokes Equations in Frequency Space, PhD Thesis, Technical University of Munich, (2014).
10. Cremer, L., Über die akustische Grenzschicht vor starren Wänden, *Archiv der elektrischen Übertragung*, **2**, (1948).
11. Oschwald, M.; Faragó, Z.; Searby, G.; Cheuret, F., Resonance Frequencies and Damping of a Combustor Acoustically Coupled to an Absorber, *Journal of Propulsion and Power*, Vol. 24 (3), (2008).